Received: 12 August 2020 | Revised: 2 April 2021 | Accepted: 11 May 2021

DOI: 10.1002/stc.2800

RESEARCH ARTICLE

WILEY

Optimal design of the ideal grounded tuned mass damper inerter for comfort performances improvement in footbridges with practical implementation considerations

Maurizio De Angelis | **Francesco Petrini** | **Daniele Pietrosanti**

Department of Structural and Geotechnical Engineering, Sapienza University of Rome, Rome, Italy

Correspondence
Francesco Petrini, Department of Structural and Geotechnical Engineering, Sapienza University of Rome, Rome, Italy.
Email: francesco.petrini@uniroma1.it

Funding information
Sapienza Università di Roma, Grant/Award Numbers: RM11715C8262BE71, RP1181643697C751

Summary

The paper focuses on the optimal design of the grounded tuned mass damper inerter (TMDI) in footbridges and on some practical implementation issues. An optimal design procedure is implemented for the perfectly grounded ideal TMDI (infinite stiffness of the connection at the ground plus linear and non-dissipative inerter). The procedure is based on reduced-order models of the footbridge by assuming the frequency ratio and damping factor as design parameters, for a given number of values of the TMDI the inertance and mass ratios aiming at minimizing the maximum acceleration response of the system for users' comfort improvement under performance criteria defined in Human-induced Vibration of Steel Structures (HiVoSS) guidelines. The procedure is applied to an existing footbridge suffering excessive human-induced vibrations. After the optimal design of the TMDI has been found, its performances are assessed by the avail of a fully 3D finite element model of the case-study footbridge, which has been calibrated toward an in situ experimental identification campaign. Alternative proposals for practical implementation of the control system are analyzed. Finally, a performance sensitivity analysis is carried out regarding the deviations from the initial assumption of perfectly grounded TMDI system, by varying the stiffness of the connection at the ground of the ideal inerter. Results show that the proposed procedure makes the TMDI a very efficient control system for footbridges and that changes of the stiffness of the grounded connection drop the beneficial effect of the TMDI, also if consequences of such errors are less than the ones occurring in classical TMDs for detuning or malfunctioning.

KEYWORDS

comfort, footbridges, optimal design, TMDI, vibration control

1 | INTRODUCTION

Limiting excessive accelerations in vibrating behavior of footbridges is one of the main design issues for this kind of structures.[1] In fact, many of the built footbridges have very low damping ratios and stiffness, and they exhibit natural mode shapes falling in the range of frequencies that are critical for human vibration perception due to excessive human-induced vertical acceleration of the deck, something often causing discomfort in users during service.[2] Furthermore, a peculiar characteristic of problems related with slightly damped structures, is that multiple modes and frequencies can contribute to the total peak response experimented by the structure, something that is especially true for accelerations. In order to ensure user comfort and safety, many footbridges today are equipped with tuned mass dampers (TMDs).[3,4] Nevertheless, since the TMD is effective is suppressing only the contribution to the vibrations of the specific frequency which it is tuned with, its effectiveness in improving vibrations comfort performances of footbridges can be limited by the broadness of the spectral frequency range characterizing the human-induced vibrations. Due to this broadness in fact, it can occur than more than one footbridge's mode falls in the human-induced vibrations frequency range, something requiring a multimodal performance assessment procedure. In addition to this, applications of TMDs in slender structures can be, in general, prevented by the large amount of secondary mass (mass of the TMD) that would be required by the device to be effective. Furthermore, uncertainties affecting the dynamic characteristics of the structure in its "as-built" configuration (e.g., uncertainties affecting the structural damping or natural frequencies) can lead to the detuning of the designed TMD, something that dramatically drops the TMD effectiveness.[5] Alternative devices with some potential for multimodal vibration control have been recently proposed in literature to improve the performances of classical TMDs, but their development is currently still focused on single-mode control.[6]

Among different alternative technologies aiming at performing better than classical TMDs, inerter-based vibration control devices became very popular in the last 5 years in the Civil Engineering field. The inerter is a two-terminal device that resists to relative accelerations (a_2–a_1) between its terminals,[7] which can be realized with different technologies as, for example, (i) mechanical inerters,[8] (ii) hydraulic inerters,[9] and (iii) electromagnetic inerters.[10] In its ideal configuration, the resistance force produced by an inerter is directly proportional to (a_2–a_1) via a constant b named *inertance* and expressed in kilograms. The tuned mass damper inerter (TMDI) is one of the most general configurations of such inerter-based control systems, whose rheological model is shown in Figure 1a.

Introduced by Marian and Giaralis in 2014,[11] the TMDI is obtained by a classical TMD in which the mass is connected with one of the two terminals of an inerter, having the other terminal (k in Figure 1) grounded or attached to other parts of the primary structure to be controlled. The way that the inerter is connected by its k terminal to the ground g (or to the rest of the structure) is generally considered as *perfect*, in the sense that the stiffness of the connection to the ground is infinite. Most of the literature applications focuses on the so-called *perfectly grounded* inerter or TMDIs (terminal k in Figure 1a is rigidly connected to, or is coincident with, the ground g, which is considered having infinite stiffness). If the perfectly grounded assumption is removed (because of the stiffness of the connection to the ground or of the ground itself cannot be assumed as infinite), the rheological schematization of the *nonperfectly* grounded control system, TMDI_{NC}, has to be changed as shown in Figure 1b, where the flexibility of the connection k_G is explicitly taken into account. Such an imperfection of the grounded connection has never been considered in the literature also if it is expected to affect the effectiveness of the TMDI in suppressing vibrations.

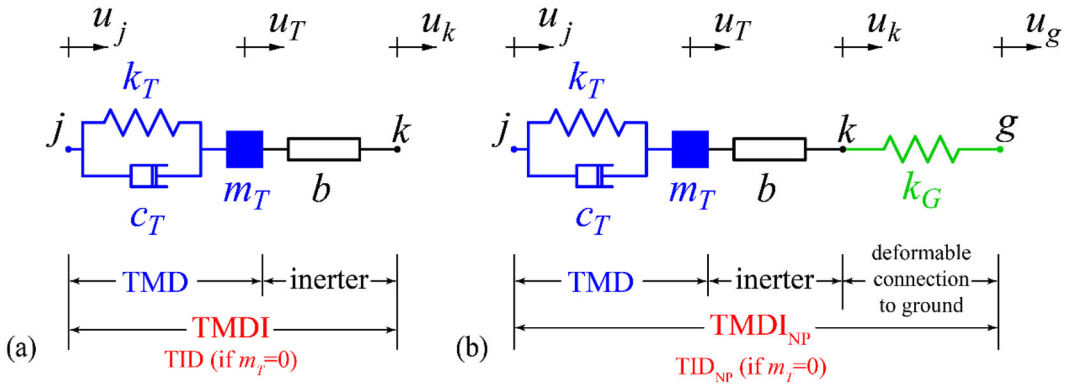

FIGURE 1 Schematic representation of the TMDI. (a) Perfectly grounded and (b) nonperfectly grounded

The above-mentioned generality of the TMDI holds in the fact that it can be downgraded to the TMD and the tuned inerter damping (TID) by assuming zero values for the inertance or for the TMDI mass, respectively. Finally, grounded TMDIs working at large inertances have shown a vibration suppression behavior that is similar to nonconventional large-mass TMDs (TMD_{NC}).[12,13]

The main skills/advantages of the TMDI with respect to the classical TMD in the field of vibration control for Civil Engineering structures are as follows:

- The inerter produces the so-called "mass amplification effect," leading to a notable difference between the inertial and gravitational mass of the control device.[14] This characteristic is relevant due to the fact that the efficiency of the TMD is, in general, proportional to the inertial mass of the device (which for classical TMDs is the same as the gravitational mass). Required TMD gravitational masses can reach unfeasible values, especially for primary structures like slender bridges or high-rise buildings where such masses have to be located at the most displaced part of the deformed structure (e.g., top floor in tall building). Being in the TMDI, the inertial "apparent" mass up to 200 times larger than the gravitational one, the same vibration suppression efficiency of large-mass TMDs, can be obtained by up to 1/200 of the gravitational mass. Lightweight TMDI devices performs as well as huge TMDs in suppressing vibrations of the mode shape for which they are tuned.
- The inerter has the capacity of exerting a certain damping effect on modes that are different from the one which the TMDI is tuned with.[15,16] This "multiple-mode suppression" effect is clear by comparing the frequency response function (FRF) or dynamic transfer function of the primary structure and of the primary structure equipped with the TMD or with the TMDI.[17] This skill of the TMDI is particularly important when more than one mode shape contributes to the relevant response of the system, as usually occurs in vibration comfort problems, which are governed by accelerations.
- The TMDI has been shown to be more robust than the TMD system to the detuning and to the other uncertainties affecting the problem parameters (e.g., eigenfrequencies, mass, external forces magnitude, and frequencies).[14,16]
- The addition of the inerter to the TMD is able to substantially drop the stroke of the TMD mass (i.e., peak relative displacement of the TMD mass with respect to the primary structure), which is an important design parameter for these kind of devices.[17,18] Large stroke can require unaffordable space allocations for the devices, especially in existing structures.

The TMDI has been studied and applied to the vibration control of a variety of Civil Engineering structural systems under different load conditions such as optimal design of perfectly grounded TMDI for SDOF systems under white or colored noise excitation,[14,18] multistory earthquake-resistant frame structures,[19,20] base isolated structures under earthquakes,[18,21] high-rise buildings under wind,[10] long-span bridges under wind,[22] and wind turbines.[23] Surprisingly, no references are found in literature regarding the application of the TMDI for vibration suppression in footbridges under human-induced loads, despite to the enhanced characteristics of the TMDI highlighted above seem really promising in addressing the limits of the classical TMD in the field.

In the best of the authors' knowledge, the only literature paper proposing a device that is similar to the TMDI for vibration suppression in footbridges is the above-mentioned work by Terrill et al,[6] where an active device named twin rotor damper (TRD) is implemented in an existing footbridge to control vibrations. The TRD is ideally able to control more than one vibration mode of the structure by appropriate calibration of the control algorithm, and the rotating masses provide some "mass amplification" effect similar to the one exerted by the inerter in TMDIs. The TMDI substantially differs from the TRD because it is a passive control device, not needing for actuators and sensors for the correct feedback operation.

In this paper, the TMDI system is optimally designed for increasing vibration comfort performances of an existing steel footbridge. After a brief panoramic view of the analysis methods and issues in design of footbridges for vibration comfort (Section 2), a framework for the TMDI optimal design for comfort improvement in footbridges is defined in Section 3 under specific simplified assumptions made for (a) dynamics of the structure, (b) human-induced loads, and (c) ideal inerter and perfectly grounded conditions. The framework is applied to an existing case-study bridge in Section 4, where the assessment of performances is carried out by a 3D finite element (FE) model; finally, in Section 5, the sensitivity of the system performances is investigated when the previously mentioned design simplified assumption of perfectly grounded connection is not verified (switching from the scheme of Figure 1a to the scheme of Figure 1b, with $k_G < \infty$). It is worth mentioning that, thanks to the data obtained by an experimental identification campaign carried out for the case-study footbridge, in the application section, a calibrated FE model of the case-study structure is used for performance assessment purposes.

Novelties of the paper with respect to the literature are about the TMDI design rather than analysis methods for comfort assessment in footbridges, which are taken from well-established and simplified methods for the design phase. Main contribution of the paper to the state of the art in TMDI design and application can be summarized as below:

1. the first application of the passive TMDI design tailored on specific design aspects for footbridges is presented herein;
2. a step-by-step general framework for TMDI optimal design in footbridges is presented and applied to a real structure toward the avail of a numerical model calibrated by field measures; and
3. a feasibility study, with pertinent considerations regarding the real implementation together with and sensitivity analysis of the TMDI performance with respect to the effectiveness (k_G stiffness) of the connection to the ground is presented.

The results provided for performance assessment purposes will be presented in the mass ratio versus inertance ratio Cartesian plane, something that will allow the reader to compare the performances of different passive control devices: TMD (zero inertance ratio), TID (zero mass ratio), TMDI (nonzero inertance and mass ratios), and TMD_{NC} (large values of the inertance or mass ratios). The main goal of the paper is to highlight the TMDI as an effective device for comfort performance improvements in footbridges, aiming at showing how the mentioned main advantages of the TMDI with respect to the conventional, TMD_C, and nonconventional, TMD_{NC}, control systems can be usefully exploited by the proposed method for suppressing excessive vertical vibrations.

2 | USERS' COMFORT PROBLEM IN THE DESIGN OF FOOTBRIDGES

Because of their slenderness, extremely low structural damping, and the frequency broadness of the human-induced excitation, footbridges are prone to undergoing human-induced perceptible vibrations in service, something that can seriously compromise the comfort of the users.[24,25] Therefore, serviceability requirements related to peak accelerations experimented by the structure under crowd load are one of the driving design requirements for footbridges. The design of footbridges for vibration comfort is not trivial due to a number of reasons and, in particular, (i) difficulty in reliably modeling crowd-induced loads and crowd behaviors (including human–human interaction [HHI]); (ii) presence of human–structure interaction (HSI) in service; and (iii) uncertainties affecting the dynamic characteristics of the structure (e.g., damping and stiffness) or affecting the walking characteristics (e.g., stepping frequency) of the users, both having relevant impact on the reliability of a priori ("as-design" configuration) response evaluations.

Due to the above considerations, predicting the dynamic response of footbridges under crowd-induced loading is an important and nontrivial aspect of the structural design, which has been widely investigated as research topic in last years (e.g., Van Nimmen et al.[26]). The dynamic of the crowd load implies complex phenomena like HHI, concerning the synchronization of different pedestrians simultaneously walking on the bridge,[27] and HSI, concerning synchronization and correlation of human-induced periodic load with the vibration frequency of the structure.[26,28] The two phenomena depend from the traffic level (amount of people) acting on the footbridge: higher occupancy is related to higher synchronization between people and to lower synchronization between users and structure.[29] Furthermore, some studies demonstrated that walking action and frequency are not deterministic but stochastic in nature,[30] and advanced loading models are available in literature for considering this aspect.[31,32]

As already said, another relevant point concerns the great amount of uncertainty related to some fundamental structural dynamic characteristics of the footbridge.[33] The structural damping, in particular, is almost impossible to be deterministically evaluated in the design phase due the lack of knowledge of many parameters that will affect it in the as-built configuration, with errors in damping ratios predictions reaching almost $\pm 30\%$ of the measured values.[1] Additional complexity related to possible errors in structural damping predictions is due to the above-mentioned multimodal contribution to the relevant response parameter (peak acceleration) of footbridge for vibration performance comfort evaluation: in fact, relevant errors in specific modal damping predictions can lead to an erroneous evaluation of the contributions to that modes to the total acceleration. Moreover, HSI can result in significant changes of the effective structural damping associated to the human–structure coupled system in vertical sway, being crowed scenarios associated to an increasing (beneficial for accelerations) effective damping,[29] especially for those modal frequencies that are close to the natural frequency of the human body and then most related with vibration perception and comfort.

2.1 | Simplified methods

Due to the above-mentioned complexities related to the detailed modeling of the coupled human–structure system, advanced models are, up to date, still under development and mainly used in research but not yet applied in practical design, where simplified load models are implemented as defined in well-established and widely used guidelines, like the Human-induced Vibration of Steel Structures (HiVoSS) (Research Fund for Coal and Steel 2008—HiVoSS).[34] The HiVoSS guidelines provide the designers with a codified simplified procedure to conduct the complete processes for vibration comfort design and assessment of footbridges. These include the action model and the structural response evaluation procedure; furthermore, appropriate comfort assessment criteria based on peak acceleration-prescribed thresholds are provided.

The HiVoSS guidelines procedure is based on a total of seven steps to be performed in order to check if a certain design configuration of a footbridge will meet the comfort criteria when vibrating. The evaluation is based on a proposed simplified methodology for the calculation of the maximum acceleration experimented by the footbridge in a number of design situations. With specific reference to the three design issues mentioned above (crown load modeling with HHI, HSI, and structural damping parameter uncertainties), in the HiVoSS, the following assumptions are made:

1. The crown is modeled by an equivalent number of perfectly synchronized (among themselves) pedestrians N_{eq}, with different numbers of pedestrians (pedestrian density d) associated to different "traffic classes (TCs)" (see Table 1), which define specific design situations to be analyzed and checked for comfort assessment:

$$\begin{aligned} N_{eq} &= 10.8\sqrt{\xi_i N} \text{ for } d < 1\frac{p}{m^2}, \\ N_{eq} &= 1.85\sqrt{N} \text{ for } d \geq 1\frac{p}{m^2}, \end{aligned} \tag{1}$$

where N is the number of pedestrians over the structure (pedestrian density d multiplied by the total surface of the deck) and ξ_i is the modal damping ratio of the ith mode shape.

2. The HSI is partially taken into account by assigning to each design situation a resonance factor $\psi_{e,h}$ (named "reduction coefficient" in the guidelines) for each direction e (being $e = vert$ or lat for *vertical* and *lateral* directions, respectively), which values are shown in Figure 2 for the vertical direction ($e = vert$) and walking pedestrians. The $\psi_{vert,h}$ defines a spectrum of frequencies that are relevant to the walking load, and that has to be considered for identifying critical mode shapes and frequencies which, toward perfect resonance with the human-induced load (conservative assumption), should be considered in comfort assessment. Then, the amplitude $q^{(i)}_{vert,eq}$ of the equivalent distributed load (N/m^2) acting on the deck in vertical direction is defined as

$$q^{(i)}_{vert,eq} = \frac{N_{eq}}{S}\alpha_{vert,h}\, G\psi_{vert,h}(f_i), \tag{2}$$

where f_i is the natural frequency of the mode i under consideration, S is the total area of the bridge deck, G is the considered value for the single pedestrian body weight, and $\alpha_{vert,h}$ is the dynamic amplification factor in vertical direction,

TABLE 1 Traffic classes for comfort assessment

TC	d people/m^2
1	0.0987
2	0.2000
3	0.5000
4	1.0000
5	1.5000

depending on the harmonic number that characterizes the considered mode shape and is taken, for the vertical direction and first harmonic, equal to 0.4.

The distribution of the equivalent load along the footbridge deck has to be applied with appropriate sign to be in accordance with the mode shape, as shown as an example in Figure 3.

3. The uncertainties related with structural damping and stiffness are not explicitly modeled, as well as the increased damping due to the HSI. On this point, the HiVoSS guidelines contain recommendations regarding both the appropriate (minimum and average) damping ratios to consider in the assessment analysis for the as-designed structure (classified by structural typology) and the procedures to put in place in order to evaluate the real dynamic properties of the as-built structure.

Under the three above-mentioned assumptions, the HiVoSS guidelines allow to conduct the comfort assessment by analyzing separately equivalent SDOFs models related with the critical mode shapes and by assuming resonant harmonic forces. The assessment is conducted by comparing the maximum accelerations experimented by the deck with prescribed ranges assigned to different comfort classes (CLs) or performance levels (see Table 2).

The simplified models proposed by the HiVoSS guidelines lead, in general, to a quite conservative design solution with respect to the ones provided by the state-of-the-art models.[35]

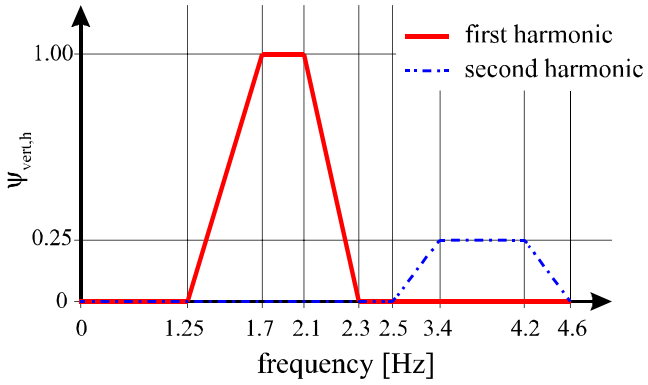

FIGURE 2 Resonance factor ("reduction coefficient") in vertical direction for walking pedestrians (after HiVoSS)

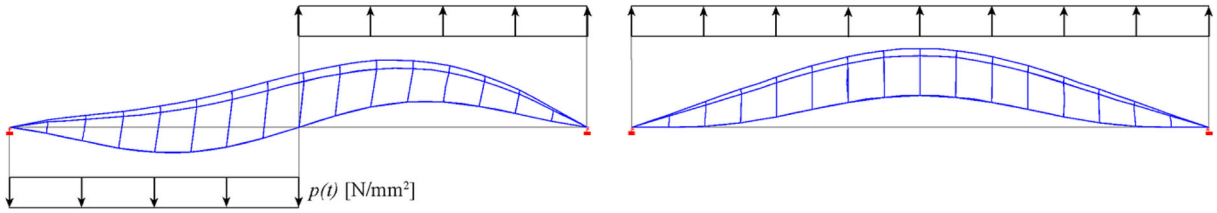

FIGURE 3 Example of the distribution of the equivalent load along the footbridge deck (after HiVoSS)

CL	Acceleration ranges	Comfort performance
1	$a_{max} \leq 0.05$ g	Maximum
2	0.05 g $\leq a_{max} \leq$ 0.1 g	Medium
3	0.1 g $\leq a_{max} \leq$ 0.25 g	Minimum
4	0.25 g $\leq a_{max}$	Inadmissible

TABLE 2 Comfort classes and acceleration ranges comfort assessment

3 | OPTIMAL DESIGN OF THE TMDI FOR ACCELERATION CONTROL IN FOOTBRIDGES

An optimal design procedure is proposed here for implementing the TMDI in footbridges prone to excessive pedestrian-induced vertical vibrations causing discomfort in users.

After a preliminary step (Step 0) where an MDOFs FE model of the footbridge is built for modal analysis purposes, the proposed procedure is articulated in the four main steps below:

1. The first step focuses on the individuation of the n mode shapes and frequencies which are potentially critical for comfort performances. This is essentially accomplished by identifying the structural eigenfrequencies that can be excited by (i.e., are resonant with) typical human-induced actions and are relevant for the vibration perception.
2. The second step is about the optimization of the TMDI design parameters (details are provided in the next section). This step implies the definition and optimization of n generalized SDOF + perfectly grounded ideal inerter models. The generalized SDOFs are representative of the above-identified mode shapes and are defined by established procedures.[36] Simplified action models are adopted, and the structural analyses are conveniently conducted in the frequency domain. The inerter here is assumed to have an ideal behavior.
3. The third step is about the assessment of the performances of the previously obtained n TMDI solutions with reference to the global MDOF model of the footbridge equipped with the TMDI. In this assessment phase, the simplified assumptions made above (e.g., ideal inerter and perfectly grounded TMDI) can be gradually removed.
4. The last step regards the selection of one of the n TMDI design solutions tested above on the basis of performance and feasibility criteria.

The proposed procedure for the optimal design of the grounded TMDI for acceleration control in footbridges is schematically described by the flowchart shown in Figure 4.

The following notes apply to the procedure:

- In order to complete the individuation of the n mode shapes at Step 1, an appropriate frequency spectrum for the human-induced actions is needed: here, without any loss of generality, reference to the frequency spectra provided by the HiVoSS for the reduction coefficient $\psi_{vert,h}$ is made for this purpose.
- At Step 2, the n SDOF + perfectly grounded TMDI (total of 2-DOF) performance-based optimization procedure is conducted as described in the following sections. A total of n cases (as many as the ones representing the mode shapes identified as potentially critical for comfort in previous steps) are analyzed/optimized. At the end of this step, n (sub)optimal TMDI design solutions are obtained.
- As will be detailed in the next section, it is expected that damping-related uncertainties will not substantially affect the SDOF-based optimization procedure.
- As already said, the simplified assumptions made in previous steps can eventually be removed at Step 3. With this purposes, a sensitive analysis can be conducted in order to investigate the impact of such simplified assumptions on the performances. Two common assumptions usually made in TMDI-equipped systems and which impact on performances are those regarding the modeling of ideal (linear and without damping) inerter and perfectly grounded TMDI (e.g., a very large value of k_G, at limit infinite).
- Step 4 regards the selection of one of the n TMDI design solutions tested above. The selection criteria should be based on both performance and feasibility/constructability considerations about the analyzed configurations. Including such a kind of consideration is important since it would be not easy to realize a perfect (very large k_G stiffness) grounded TMDI for horizontal structures like footbridges, and on the other hand, nongrounded inerter solutions are supposed to be less efficient that the grounded one.

This paper applies all the steps of the procedure. Without any loss of generality, some of the components used in Steps 1 and 2 are based on the indications contained in the HiVoSS, with particular reference to the simplified action models, the load cases to be examined in terms of TCs ("design situations"), and the acceleration thresholds to be respected for the verification of comfort. In addition, still without loss of generality, HSI is neglected in this study for simplification purposes.

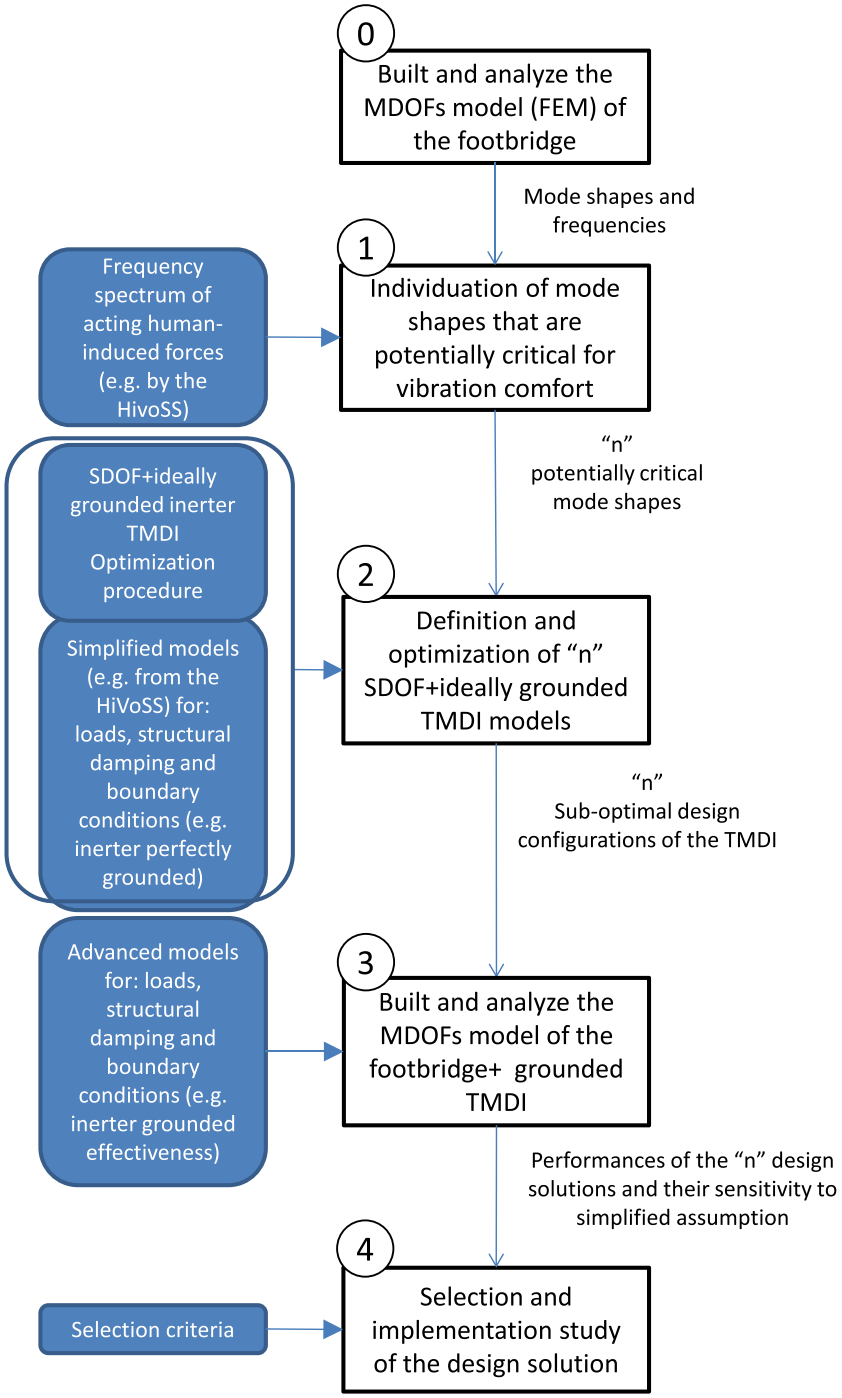

FIGURE 4 Flowchart of the proposed procedure for optimal design of the grounded TMDI in footbridges

3.1 | Step 2: Optimal design

The model used in the optimization step can be represented by the 2-DOF system shown in Figure 5, where the primary structure is represented by a mass m_I, while the TMDI is characterized with a gravitational mass m_T and is perfectly grounded (infinite stiffness of the restrain of the second inerter terminal), the primary mass is subjected to the sinusoidal force $p(t)$ representing the human-induced load. Equations of motion of such a system are derived in Appendix A of the paper and given in Equation 3.[14,18]

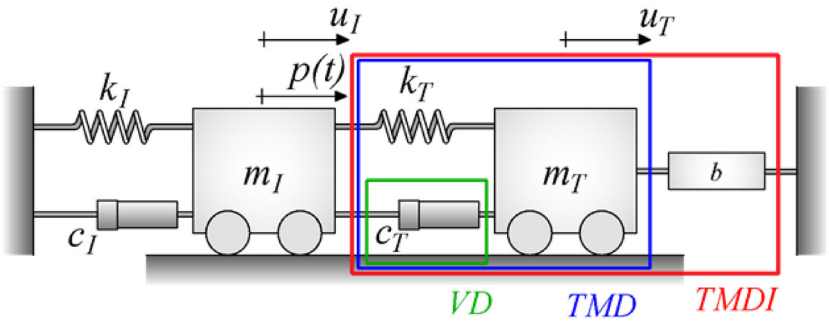

FIGURE 5 2-DOF system for grounded TMDI optimal design

$$\begin{bmatrix} 1 & 0 \\ 0 & \mu \end{bmatrix} \begin{bmatrix} \hat{A}_{u_I} \\ \hat{A}_{u_T} \end{bmatrix} + 2\omega_I \begin{bmatrix} \xi_I + \xi_T \mu_e \nu_T & -\xi_T \mu_e \nu_T \\ -\xi_T \mu_e \nu_T & -\xi_T \mu_e \nu_T \end{bmatrix} \begin{bmatrix} \dot{u}_I \\ \dot{u}_T \end{bmatrix} + \omega_I^2 \begin{bmatrix} 1 + \mu_e \nu_T^2 & -\mu_e \nu_T^2 \\ -\mu_e \nu_T^2 & \mu_e \nu_T^2 \end{bmatrix} \begin{bmatrix} u_I \\ u_T \end{bmatrix} = \begin{bmatrix} \frac{1}{m_I} \\ 0 \end{bmatrix} p(t), \tag{3}$$

where

$$\omega_I = \sqrt{\frac{k_I}{m_I}}, \quad \xi_I = \frac{c_I}{2 m_I \omega_I} \tag{4}$$

are the parameters of the primary structure, and

$$\omega_T = \sqrt{\frac{k_T}{m_T + b}}, \quad \xi_T = \frac{c_T}{2(m_T + b)\omega_T}, \tag{5}$$

$$\mu = \frac{m_T}{m_I}, \quad \beta = \frac{b}{m_I}, \quad \mu_e = \mu + \beta, \quad \nu_T = \frac{\omega_T}{\omega_I} \tag{6}$$

are the parameters of the control system. In previous equations, u_I and u_T are the displacement of the primary and secondary mass, b is the inertance constant, and ν_T and ξ_T are the TMDI frequency and damping ratios. The mass m_I and the stiffness k_I are calibrated in order to be representative of the mode shape $\phi(x,y)$ examined for the primary structure.

As already said, in the optimal design phase, the external force is taken as sinusoidal kind as indicated by HiVoSS guidelines, then as reported below:

$$p(t) = p_0 \sin(\Omega t), \quad p_0 = \boldsymbol{\phi}^T \mathbf{B}_f \mathbf{f}, \tag{7}$$

where Ω is set equal to the frequency of the analyzed mode shape of the structure without any control device (resonant condition) and p_0 is the distribution of the equivalent load provided by the HiVoSS along the footbridge deck.

To explore the full potential of the TMDI as a motion control solution for human-induced vibrations of slender footbridges, a novel optimization problem is herein formulated and solved numerically to tune TMDI parameters for users' vibration comfort. The goal is to minimize, as objective function (OF), the main peak of the acceleration's FRF $H_A^{(i)}$ of each previously defined n SDOFs equipped with TMDI systems, $\text{OF} = \left| H_A^{(i)} \right|_{\max}$, with $i = 1,2, \ldots, n$, when subjected to the considered load provided by the HiVoSS. The considered optimal design problem involves four independent design

parameters, namely, the TMDI frequency and damping ratios ν_T and ξ_T defined above, and grouped in the vector $\mathbf{x}_1 = [\nu_T\ \xi_T]^T$, as well as the mass and inertance ratios (also already defined) μ and β, grouped in the vector $\mathbf{x}_2 = [\mu\ \beta]^T$. The optimization problem is solved numerically using standard "pattern search" algorithm in MATLAB® to determine optimal design parameters in $\mathbf{x}_1$ (primary design parameters) bounded within a prespecified search range $\mathbf{x}_1^{\min}$ and $\mathbf{x}_1^{\max}$ for different given values of the parameters in $\mathbf{x}_2$ (secondary design parameters). The above is mathematically written as

$$\min_{\mathbf{x}_1}[OF(\boldsymbol{x}_1|\boldsymbol{x}_2)] \text{ subjected to } \mathbf{x}_1^{\min} \le \mathbf{x}_1 \le \mathbf{x}_1^{\max}, \tag{8}$$

where the range of values of both primary and secondary design parameters has to be chosen to ensure practically feasible configurations. Note that the above optimal design formulation allows for explicit treatment of the TMD (conventional, TMD_C, and nonconventional, TMD_NC) and the TID as special cases of the TMDI by taking $\beta = 0$ or $\mu = 0$, respectively.

This way of handling the inertance ratio as secondary design parameter in optimal TMDI design problems is quite common in the literature and has been adopted also in previous works of the present authors.[16–18] On the basis of the experience accumulated by the authors on this specific topic, this approach allows to avoid convexity problems in the OF, which usually rise up when β is considered as a primary design variable.

It is worth to motivate the choice of conducting the optimal design by making use of generalized SDOF models of the primary footbridge structure: for SDOF models, the optimal values of the primary design parameters obtained with the procedure will be *independent* from the value of the modal structural damping assumed for the primary system during the calculations and will be the same for any value of the structural (modal) damping. Consequently, the optimal primary design parameters will be not affected by the large amount of uncertainty affecting the structural damping itself. The last would be not true in case the optimization is conducted by MDOF models of the primary structure, where errors/uncertainty affecting the relative values between the modal damping of involved modes (e.g., correct estimation of the first modal damping and erroneous value of the second modal damping) would lead to erroneous optimal values for the primary design parameters. Then, by operating with SDOF models of the footbridge structure at this stage, we can prevent the negative circumstance where optimal design variables are not correct due to an error in setting the value of the structural damping of the footbridge.

3.2 | Step 3: TMDI performances assessment by the MDOFs model

After the optimization of the control system has been conducted by a simplified SDOF + perfectly grounded control system subjected to sinusoidal load, the performances of the footbridge equipped with TMDI are assessed by a complete 3D model, where the simplified assumptions made in previous steps (e.g., perfectly grounded TMDI) can be eventually removed.

Due to the current unavailability of appropriate FEs to model the inerter (i.e., FE members resisting to the relative accelerations between the two terminals), the complete 3D model of the footbridge equipped with the TMDI can be obtained by modifying the stiffness, mass, and damping matrices (i.e., by adding an additional row and line to the matrices) of the primary structure as extracted from a complete FE model of the uncontrolled footbridge and then obtaining the "expanded" system matrices which consider the primary structure equipped with the TMDI.[11] In particular, if the lumped mass approximation is made for the FE model of the primary structure, when an ideal, perfectly grounded, and punctually connected TMDI with inertance b, gravitational mass m_T, stiffness k_T, and damping coefficient c_T, is connected to the jth DOF of the footbridge, the additional diagonal element of the expanded mass matrix $\mathbf{M}$ is equal to m_T+b. Both diagonal and out-of-diagonal modifications occur to the stiffness and damping matrices $\mathbf{K}$ and $\mathbf{C}$. The elements corresponding to the jth DOF are simply changed in k_j+k_T and c_j+c_T, being the additional diagonal element of the expanded matrices equal to k_T and c_T respectively. The stiffness and damping coefficients of the TMDI also appear in the added column and row in correspondence with the jth row and column, respectively. Examples of the above-described mass, stiffness, and damping expanded matrices for an n-DOF footbridge equipped with a TMDI are shown in Equation 9.

$$\boldsymbol{M}=\begin{bmatrix} m_{11} & \cdots & 0 & \cdots & 0 & 0 \\ & \ddots & \ddots & \ddots & \ddots & \vdots \\ & & m_{jj} & \ddots & \ddots & 0 \\ & & & \ddots & \ddots & \vdots \\ & SYM & & & m_{nn} & \vdots \\ & & & & & m_T+b \end{bmatrix},$$

$$\boldsymbol{K}=\begin{bmatrix} k_{11} & \cdots & k_{1j} & \cdots & k_{1n} & 0 \\ & \ddots & \ddots & \ddots & \ddots & \vdots \\ & & k_{jj}+k_T & \ddots & \ddots & -k_T \\ & & & \ddots & \ddots & \vdots \\ & SYM & & & k_{nn} & \vdots \\ & & & & & k_T \end{bmatrix}, \tag{9}$$

$$\boldsymbol{C}=\begin{bmatrix} c_{11} & \cdots & c_{1j} & \cdots & c_{1n} & 0 \\ & \ddots & \ddots & \ddots & \ddots & \vdots \\ & & c_{jj}+c_T & \ddots & \ddots & -c_T \\ & & & \ddots & \ddots & \vdots \\ & SYM & & & c_{nn} & \vdots \\ & & & & & c_T \end{bmatrix}.$$

In Equation 9, m_{rq}, k_{rq}, and c_{rq} (with $r,q = 1,2, ..., n$) represent the elements of the mass, stiffness, and damping matrices of the n-DOF footbridge FE model without the TMDI.

4 | APPLICATION TO A CASE STUDY ON AN EXISTING FOOTBRIDGE

The case study is the footbridge on the Velino River in Rieti (Italy), built on the occasion of the athletic junior championships, held in June 2013 in the city, in order to create a direct cycle-pedestrian link between the Velinia road and the athletics stadium. The bridge has a steel structure with a lower path system. The supporting structure of the bridge, which is intended for cycle-pedestrian traffic with a deck width of 3.80 m, consists of two steel arch tubes, while the transverse structure that connects the two tubes is made with a network of beams HEA 220. The two lateral support arches are inclined of 38° with respect to the vertical plane toward the outside, have a maximum arrow of 4.30 m, and are made with tubular of 406-mm diameter. To contrast the effects of geometric nonlinearity, the two arches are stiffened by the presence of a second arch, on each side, with a diameter of 219.1 mm connected to the main by steel elements HEA 220 elements. The arch foundation is on piles. The deck support system is realized by eight elastomeric FIP SI-S350/75 bearings type, four of them positioned in the pinned joints of the two main lateral arches and four positioned in the arrival points of the horizontal current tubulars. Pictures and details on the structure are shown in Figures 6 and 7.

Since from its early opening to service, the footbridge suffered from perceptible vibrations induced by pedestrians, something that suggested the owner to start a structural monitoring/identification campaign for assessing causes and finding proper solution to mitigate these vibrations and then increasing the comfort performances. A multichannel acquisition system by HBM has been adopted. It consists of a data acquisition unit McGill's interfaced with the software

FIGURE 6 Picture view of the footbridge over the Velino River

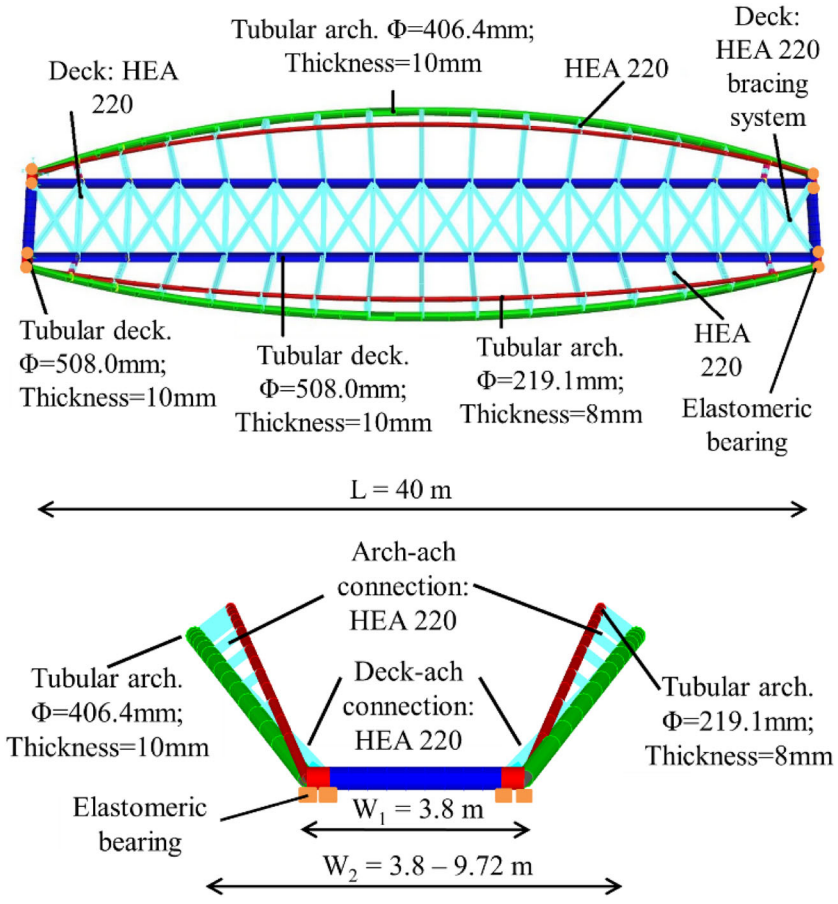

FIGURE 7 Footbridge over the Velino River: FE model and details of structural elements. Plan view (upper); cross section (bottom)

Catman Professional 5.0. The acceleration time histories are recorded using piezoelectric accelerometers by PCB Piezotronic, series 393A03, with a sensitivity of 1000 mV/g. Several ambient vibration test (AVT) campaigns have been performed, and different sensor configurations have been considered. The identification campaign leads to a number of data regarding structural eigenmodes and eigenfrequencies and structural damping for the footbridge, which were used for the calibration of a FE model of the structure.

4.1 | Mode shape selection for TMDI optimization

The selection of mode shapes that are potentially critical for comfort is carried out with reference to the vertical displacement direction of the deck and by selecting the mode shapes having eigenfrequencies falling inside the spectrum of the human-induced dynamic actions provided by the HiVoSS guidelines for walking pedestrians (see Figure 2). The mode shapes individuated as potentially critical are shown in Figure 8 and listed in Table 3, together with the indication of the most displaced location and frequencies, which are also superimposed to the load spectrum for walking pedestrians.

For the first and the third selected mode shapes (Modes 2 and 4), the maximum vertical response is located at midspan ($L/2$), while for Mode 3, the maximum vertical response is at $L/4$, where L is the span of the bridge. In terms of resonance, with reference to the walking pedestrians, Mode 4 is the one associated with the highest resonance factor (equal to 0.25). It is also worth noting that there are big differences between the three structural modal damping (identified by the above-mentioned field experimental campaign), something highlighting the above-mentioned need of having an optimal design procedure which is independent from this parameter.

The performance of the footbridge in term of occupants comfort is evaluated in what follows with reference to the only walking pedestrians' spectrum and by comparing the peak vertical accelerations of the deck as experimented under simplified model of the human-induced actions with guideline-prescribed threshold values depending, as said above, on CL levels related to the footbridge.

4.2 | Optimal single-mode design of the TMDI

The optimization of the TMDI design parameters is carried out as described above and for the identified mode shapes. As highlighted in Section 3.1, the range of values of both primary and secondary design parameters has to be chosen to

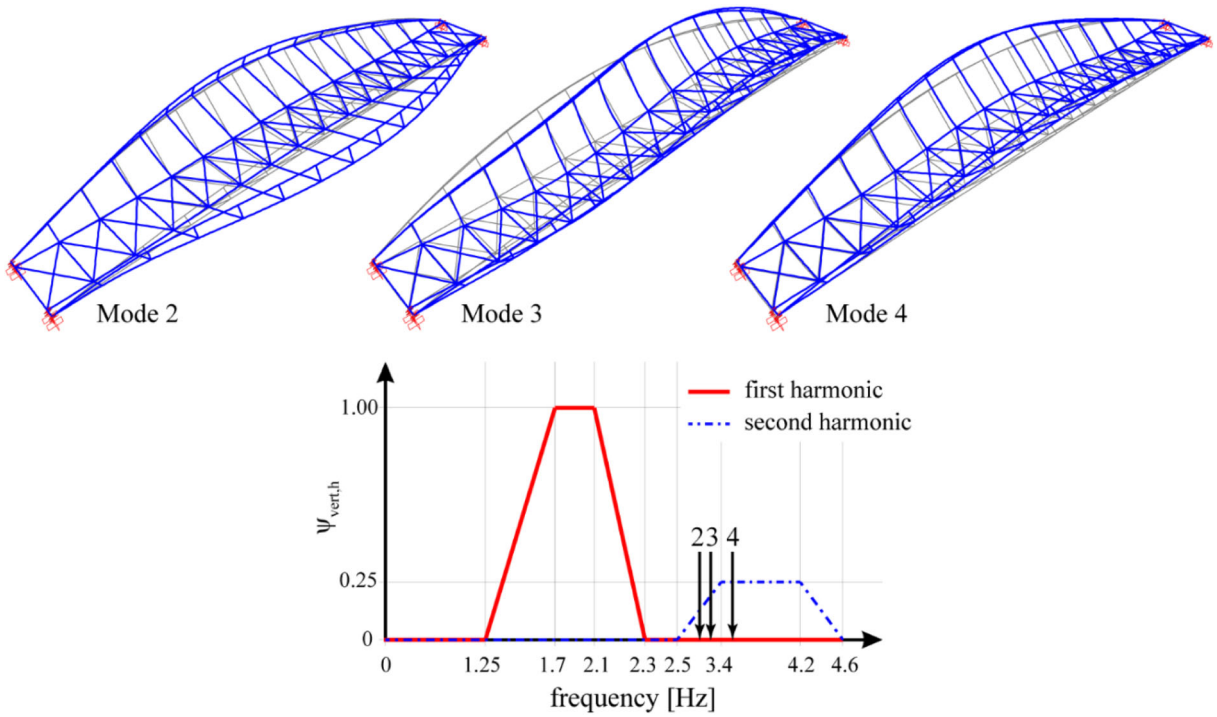

FIGURE 8 Critical mode shapes for comfort and superposition of the eigenfrequencies with the HiVoSS load spectrum

TABLE 3 Critical mode shapes for comfort

Mode No.	Freq (Hz)	ξ (%)	Max vertical response
2	2.982	0.14	$L/2$
3	3.256	1.17	$L/4$
4	3.774	0.43	$L/2$

ensure practically feasible configurations; to this end, the upper bounds of ν_T and ξ_T are set equal to 1.2 and 0.8, respectively, on the basis of considerations related with the necessity of maintaining the gravitational mass of the TMDI under a reasonable threshold for not influencing the slenderness and the static deformation of the structure. Then, in all the ensuing numerical work, the search range used in solving Equation 8 is taken as $\mathbf{x}_1{}^{\min} = [0.2\ 10^{-5}]^T$ and $\mathbf{x}_1{}^{\max} = [1.2\ 0.8]^T$. From a computational viewpoint, strong convex behavior of the OF on the primary design variables ν_T–ξ_T plane is noted with a single global optimal design point being observed for all TMDI optimization cases considered.

For illustration, Figure 9 plots the normalized OF for Mode 4 ($\left|H_A^{(4)}\right|_{\max} / \left|H_A^{(4)}\right|_{\max,NC}$ with NC meaning "no control") in the primary design variables space for fixed μ and β values to demonstrate the typical level of convexity and stable convergence of the optimization problem in equation.

As an example of the optimization results, the SDOF not controlled model (NC) for Mode 4 and the SDOF + TMDI model in its optimal configuration $\mathbf{x}_1{}^T = [\nu_{Topt}\ \xi_{opt}]^T = [0.91\ 0.28]^T$ for the case $\mathbf{x}_2{}^T = [\mu\ \beta]^T = [0.001\ 0.2]^T$ are compared in Figure 10 in terms of normalized FRFs for displacement and acceleration. The optimization procedure leads to a Den Hartog's kind of configuration for accelerations, where the two peaks of the absolute FRF are dropped almost at the same value, with a certain shift to the left of the FRF, while for displacements, also if the FRF does not present the typical shape of the Den Hartog's optimization because performances are optimized for accelerations, it is significantly dropped.

The evolution of the acceleration normalized FRF for the same SDOF + TMDI system for a fixed ν_{Topt} and different values of ξ_T is shown in the left-side column of Figure 11a,c,e for the considered modes, which in figures are ordered from the top to the bottom accordingly with increasing structural damping (the pertinent mode is indicated in the panel). The evolution of the same normalized FRF for the case where ξ_T is fixed to the ξ_{opt} value and ν_T varies is instead shown in the right-side column of Figure 11b,d,f. The following general consideration can be made regarding these FRFs:

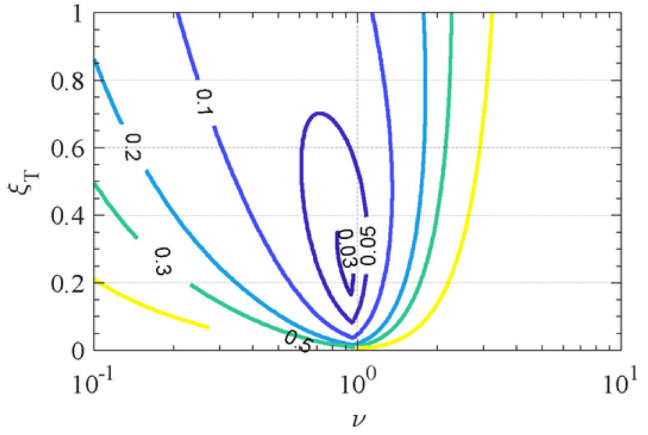

FIGURE 9 Normalized objective function versus design parameters ν_T and ξ_T for Mode 4 ($\mu = 0.001$, $\beta = 0.2$, and $\xi_I = 0.043$)

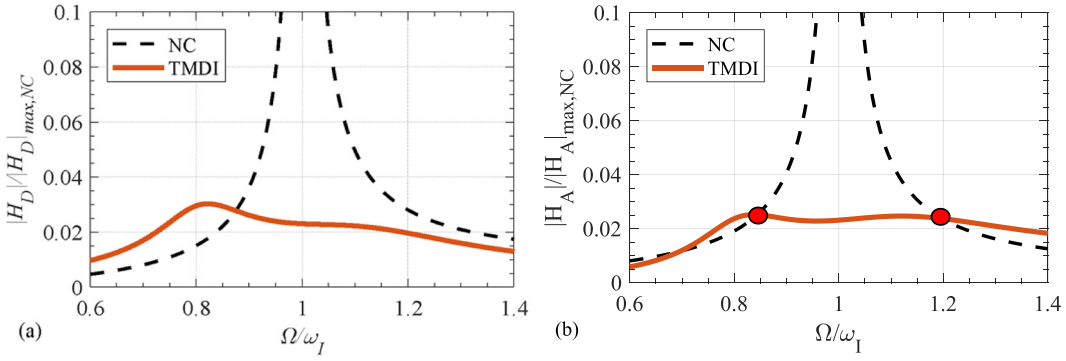

FIGURE 10 Comparison between the normalized FRFs of the SDOF (Mode 4) and of the SDOF + TMDI optimized for the case $\mu = 0.001$ and $\beta = 0.2$. (a) Displacements and (b) accelerations

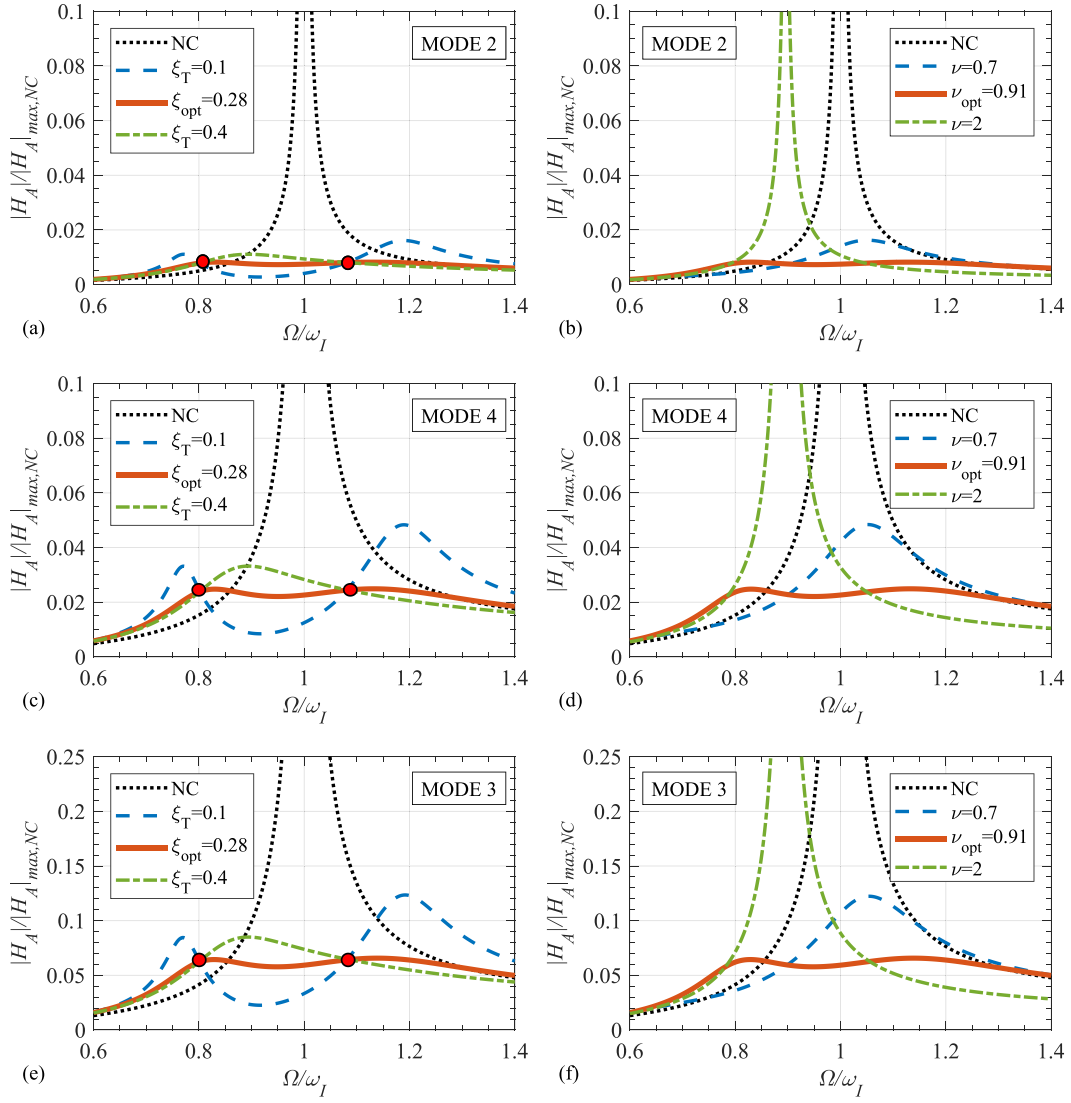

FIGURE 11 Case $[\mu, \beta] = [0.001, 0.2]$. Normalized FRF for the (a,b) SDOF (Mode 2, $\xi_I = 0.0014$) + TMDI system; (c,d) SDOF (Mode 4, $\xi_I = 0.0043$) + TMDI system; and (e,f) SDOF (Mode 3, $\xi_I = 0.0117$) + TMDI. $\nu_T = \nu_{opt}$ and varying ξ_T (left-side column); $\xi_T = \xi_{opt}$ and varying ν_T (right-side column)

- All the curves shown in the same column of Figure 11a,c,e pass through the same two fixed points, confirming that the proposed optimization leads to the typical Den Hartog's trends for the FRF evolution.
- The optimal values of the primary design parameters are independent from the damping factor of the considered mode and are equal to $\nu_{opt} = 0.91$, and $\xi_{opt} = 0.28$ for all modes.
- If, for the generic mode shape i, the ratio $\left|H_A^{(i)}\right|_{\max} / \left|H_A^{(i)}\right|_{\max,NC}$ is interpreted as a vibration suppression performance index for the TMDI, it can be observed that the peak of this performance index decreases when the modal damping increases.

The dependence of the optimal value of the primary design parameters, ν_{Topt} and ξ_{opt}, to the values assumed secondary parameters, μ and β, is shown in Figure 12, where is it shown that, by increasing the μ and β values, the ν_{opt} and ξ_{opt} values decrease and increase, respectively, something that was expected a priori, due to the conventional definitions of the design parameters provided above (e.g., inertance b is at the denominator in the definition of ξ_T).

Finally, the values of obtained peaks for the normalized FRF in optimized configurations for Modes 3 and 4 at different values of the secondary parameter $\mathbf{x}_2 = [\mu\ \beta]^T$ are shown in Figure 13. From the trends observed in this figure, it is clear how very low values of β are enough to obtain (by the simplified models used in this optimization step) peak

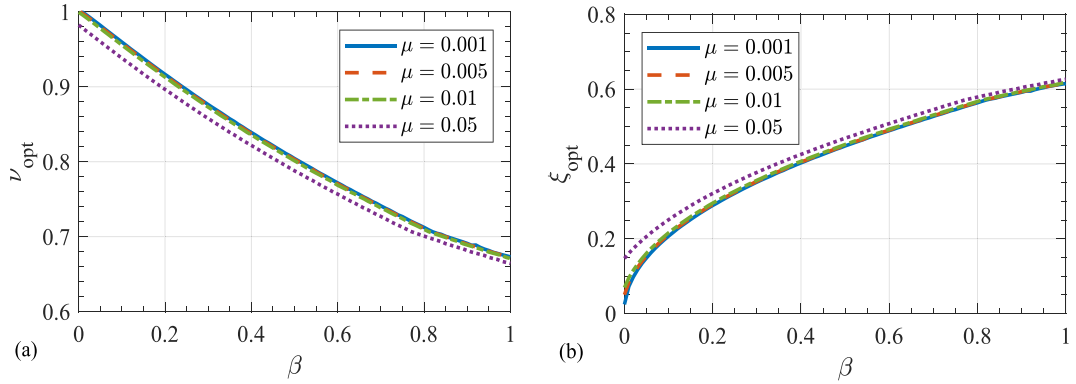

FIGURE 12 Dependence of the optimal primary design parameters to the values assumed by the secondary design parameters

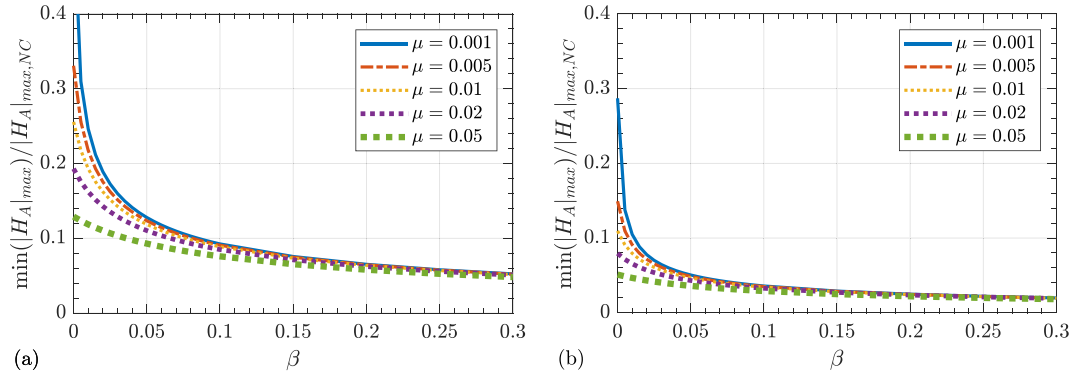

FIGURE 13 Trend of the normalized peak values of the FRFs obtained with optimal TMDI configurations obtained for different values of the secondary parameter $\mathbf{x_2} = [\mu\ \beta]^T$: (a) Mode 3 ($\xi_I = 0.0117$ and peak vertical response at $L/4$) and (b) Mode 4 ($\xi_I = 0.0043$ and peak vertical response at $L/2$)

accelerations that are lower with respect to the NC case. Figure 13 also allows for the comparison between different passive control systems that can be obtained as limit downgraded cases of the TMDI: $\mu \neq 0$ and $\beta = 0$ mean, for different mass ratio, conventional ($\mu = 0.005$–0.01) and nonconventional ($\mu = 0.02$–0.05) TMD, while $\mu = 0.001$ and $\beta \neq 0$ mean very low-mass TMDI, which is almost a TID system, at different inertances. It is shown that the presence of a certain mass is quite beneficial to the performances, especially at lower betas, where the steepness of the curves is higher. It is also clear how, for a nonconventional TMD ($\mu = 0.05$), the incremental improvements of performances obtained by adding the inertance is negligible.

4.3 | MDOF performances assessment of the TMDI-equipped footbridge

The performances of the TMDI optimized configurations obtained in previous step are assessed here by a 3D MDOF/multimodal model of the footbridge equipped with the control device.

In order to maximize the specific mode control, the TMDI has to be connected with the structure at the node where the modal displacement is maximum, being the other terminal of the TMDI rigidly (perfectly) connected to the ground. This is also what has been implicitly assumed in the optimization step, where the TMDI is connected, at one end, to the oscillating primary SDOF mass representing the single mode of the primary structure. For the considered footbridge, in order to realize a perfect grounded TMDI suppressing vibration contribute of the three considered mode shapes, appropriate footbridge–TMDI connection topologies have been conceived for the practical implementation of the control systems and schematically shown in Figure 14, where the diagonal elements under the footbridge deck are conceived as released from bending moment transmission at the two ends, and in the case of perfectly grounded TMDI, their axial stiffness k_G should be ideally considered as infinite, while in the case of nonperfectly grounded TMDI, they have a finite

stiffness, something that, as investigated in following Section 5, together with their angular configuration α, plays a certain role in the detriment of the TMDI performance with respect to perfectly grounded configuration.

The two connection topologies shown in Figure 14 determine the number and position of additional rows and column to be added to the **M**, **C**, and **K** matrices of the primary structure to consider the TMDI as detailed in Section 3.2.

In what follows, specific focus will be made on the assessment of the performance of the footbridge when equipped with a TMDI which is optimized for controlling Modes 4 and 3 and implemented as described in Figure 14a,b, respectively. The specific optimal configurations assessed are obtained for the values $\mathbf{x}_2 = [\mu\ \beta]^T = [0.001\ 0.2]^T$, for which both the nondimensional and dimensional values of the optimal parameters are shown in Table 4.

The displacement and acceleration FRFs of the jth DOF of the structure when equipped with an optimized TMDI are shown in Figure 15 (TMDI in topology (a) of Figure 14 and optimized for Mode 4, jth DOF is the vertical response at midspan) and Figure 16 (TMD in topology (b) of Figure 14, and optimized for Mode 3, jth DOF is the vertical response at 1/4-span). In the figures, the FRFs for the uncontrolled structure are also shown for comparison purposes.

It is clearly seen in the figures that, in addition to the mode which it is tuned with, the TMDI can suppress other (either higher or lower) modes. The fact that the TMDI has suppression effects both on right- and left-side frequencies suggests in general that optimizing for intermediate modes (e.g., not the first one as usually done for TMDs) leads to broad frequency range suppression effects, which can be beneficial for performances. In the examined case, for example, it is expected that the TMDI optimized for Mode 3 has a broader vibration suppression effect in the frequency range of interest, than the one that is optimized for Mode 2 or 4, something that is valuable for the robustness of the topology (b) in Figure 14. As already said, the multimodal suppression effect of the TMDI is especially effective on acceleration suppression and then for comfort improvement purposes.

The perfectly grounded TMDI optimized by the proposed approach is then certainly able to mitigate the maximum accelerations in the existing case-study footbridge. The increasing of performances of the footbridge due to the proposed implementation of the TMDI in terms of peak accelerations for different TCs is reported in Table 5 for the topology (a) of Figure 14 and when the TMDI is optimized for Mode 4. The same values obtained for the topology (b) of Figure 14 and when the TMDI is optimized for Mode 3 are reported in Table 6. By observing the results reported in Figures 15 and 16 and the values of the maximum accelerations of Tables 5 and 6, it is clear how the greater effectiveness of the TMDI is obtained by implementing the topology (b) of Figure 14, optimized for Mode 3.

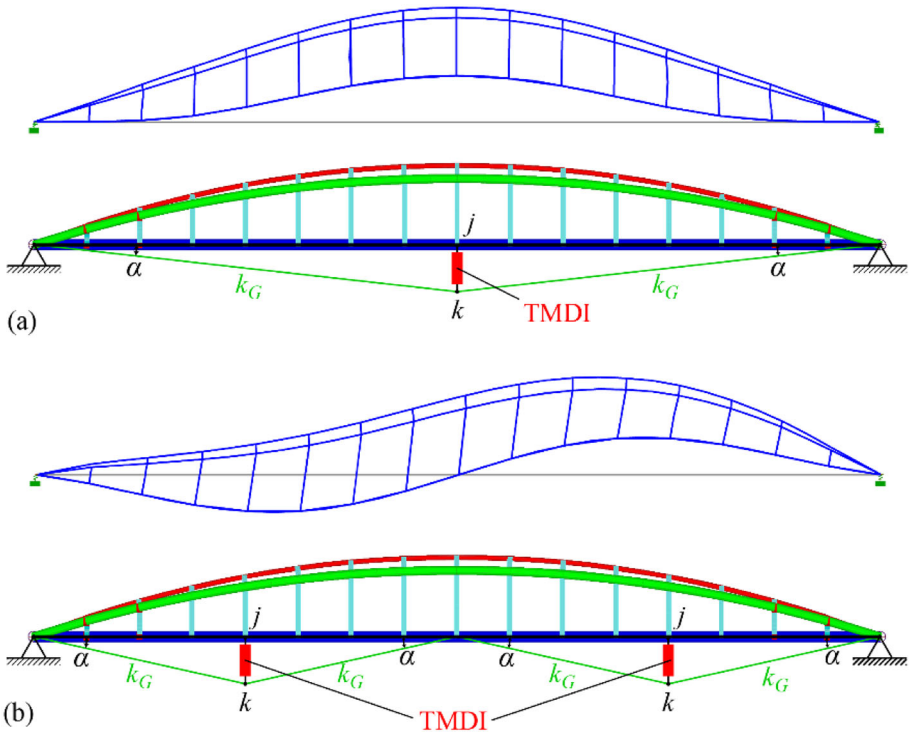

FIGURE 14 Topological connection of the grounded TMDI compared with the mode shapes to be controlled. For control of (a) Modes 2 and 4 and (b) of Mode 3

TABLE 4 Dimensional and no dimensional parameters

Parameters	Mode 4	Mode 3
SDOF system		
m_I (kg)	13109.3	21070.6
ξ_I (%)	0.43	1.17
ω_I (rad/s)	23.715	20.456
TMDI (no dimensional)		
μ	0.001	0.001
β	0.2	0.2
ν	0.91	0.91
ξ_T	0.28	0.28
TMDI (dimensional)		
m_T (kg)	13.1	21.1
b (kg)	2621.9	4214.1
k_T (kN/m)	1231.1	1472.3
c_T (kN/m)	31.2	43.3

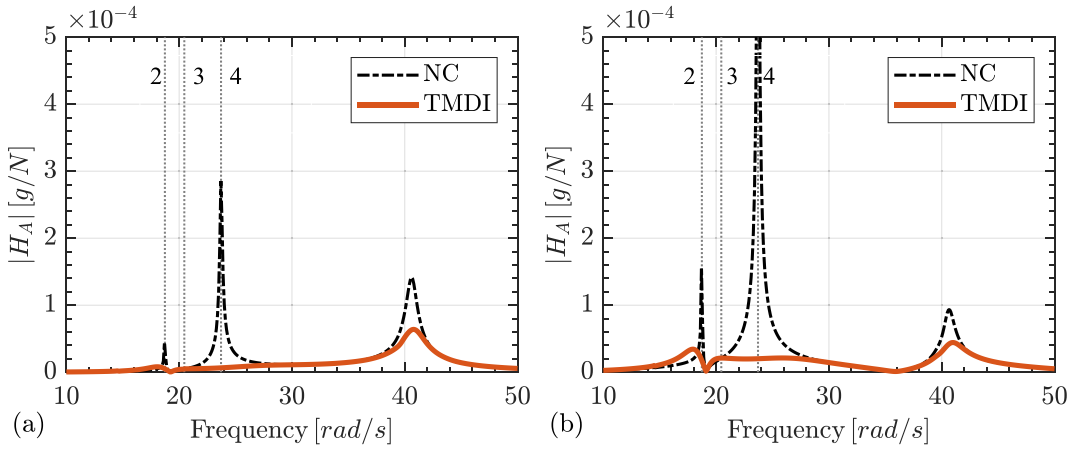

FIGURE 15 FRFs in terms of acceleration at (a) $L/4$-span and (b) midspan under a harmonic force applied at midspan for the system when the design of the TMDI is optimized for Mode 4—topology (a) in Figure 14

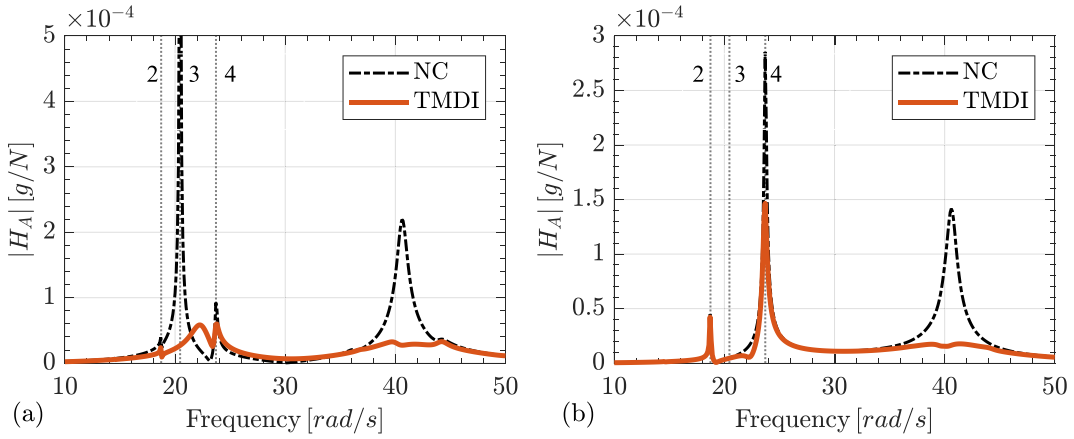

FIGURE 16 FRFs in terms of acceleration at (a) $L/4$-span and (b) midspan under a harmonic force applied at midspan for the system when the design of the TMDI is optimized for Mode 3—topology (b) in Figure 14

In order to give a broad view of the performances of the proposed TMDI system, the time histories of the accelerations of the jth DOF of the structure when equipped with an optimized TMDI are shown in Figure 17 (TMDI in topology (a) of Figure 14, and optimized for Mode 4, jth DOF is the vertical response at midspan) and Figure 18 (TMD in topology (b) of Figure 14, and optimized for Mode 3, jth DOF is the vertical response at 1/4-span), with a comparison of the same time histories as obtained for the uncontrolled structure. The time histories are obtained by a linear dynamic analysis in time domain and by applying at midspan a harmonic force which is resonant with the target mode of the optimized TMDI (i.e., Mode 4, $f_4 = 3.774$ Hz for Figure 17, and Mode 3, $f_3 = 3.256$ Hz in Figure 18).

4.4 | Some considerations regarding the practical implementation and the selection criteria of the best optimal solution

The last step of the procedure delineated in Figure 2 for the optimal design and implementation of the TMDI in footbridges prone to excessive pedestrian-induced vertical vibrations causing discomfort in users concerns the selection of the best solution between the different alternatives that emerged from previous step. Such a selection should be made not only on the basis of vibration suppression performances but also on other practical considerations, for example,

TABLE 5 Performances of the optimized TMDI (optimal design focusing on Mode 4)

	No TMDI		TMDI optimized for Mode 4	
TC	a_{max} (g)	CL (Table 2)	a_{max} (g)	CL (Table 2)
1	0.071	CL2	0.002	CL1
2	0.101	CL3	0.002	CL1
3	0.159	CL3	0.004	CL1
4	0.589	>CL4	0.015	CL1
5	0.720	>CL4	0.018	CL1

TABLE 6 Performances of the optimized TMDI (optimal design focusing on Mode 3)

	No TMDI		TMDI optimized for Mode 3	
TC	a_{max} (g)	CL (Table 2)	a_{max} (g)	CL (Table 2)
1	0.026	CL1	0.002	CL1
2	0.040	CL1	0.002	CL1
3	0.060	CL2	0.004	CL1
4	0.133	CL3	0.009	CL1
5	0.164	CL3	0.011	CL1

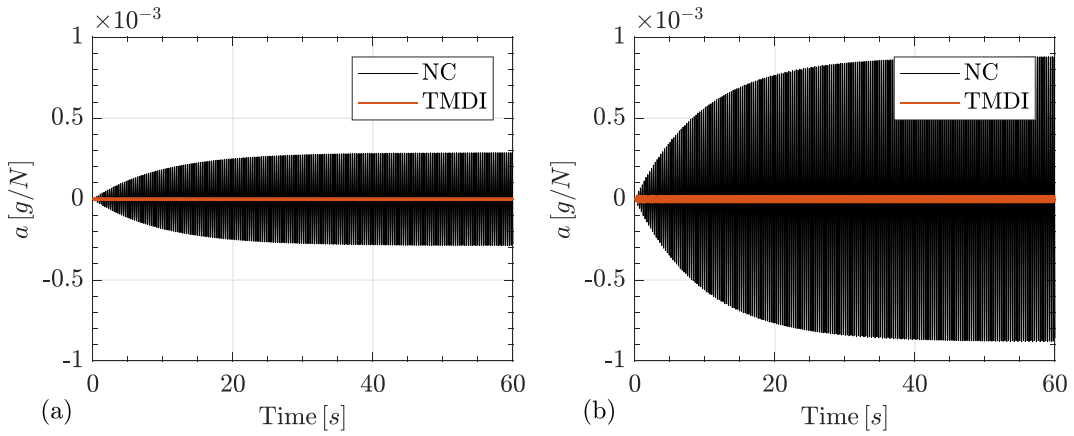

FIGURE 17 Time histories in terms of acceleration at (a) L/4-span and (b) midspan under an harmonic force ($f_4 = 3.774$ Hz) applied at midspan for the system when the design of the TMDI is optimized for Mode 4—topology (a) in Figure 14

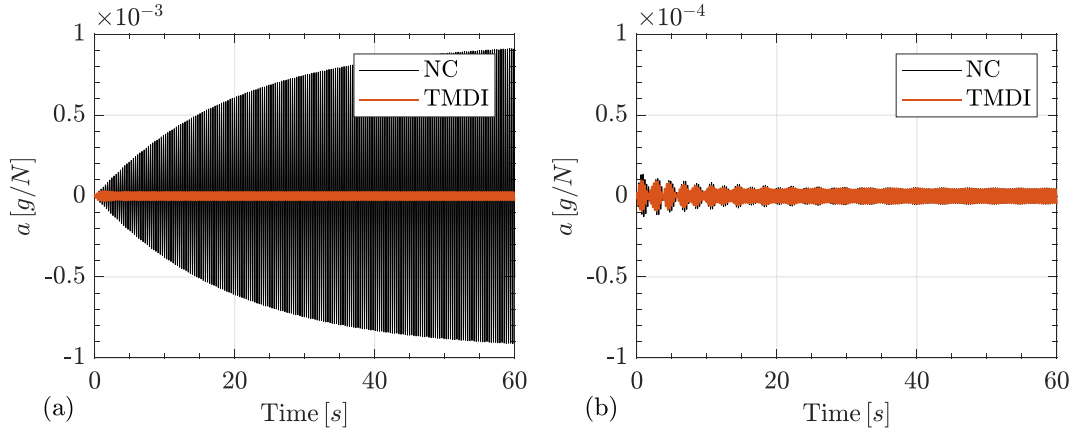

FIGURE 18 Time histories in terms of acceleration at (a) $L/4$-span and (b) midspan under an harmonic force ($f_3 = 3.256$ Hz) applied at midspan for the system when the design of the TMDI is optimized for Mode 3—topology (b) in Figure 14

- effectiveness and robustness of the system with respect to imperfection, detuning, and malfunctioning;
- realization complexity/feasibility of the proposed solution;
- costs of the proposed solution; and
- durability.

In the examined case, the two implementation topologies proposed in Figure 14 should be compared in view of all these criteria. In this work, for brevity, among the previous considerations, only the first has been deepened.

As said above, in terms of vibration suppression performances, the implementation of optimal design for Mode 3 (i.e., topology (b) in Figure 14) is the most efficient one as can be argued from Tables 5 and 6. Another positive aspect of the topology (b) with respect to (a) is that, as can be argued also from the FRFs shown above, in topology (b), the TMDI acts as vibration suppressor both for Mode 3 (for which it has been optimized) and (to some extent) for Mode 4; this is due to the fact that the j-DOF of Figure 14b are excited in both modes. The same does not hold for the topology (a), which is effective in suppressing vibrations of Mode 4 but is not in suppressing the vibrations of Mode 3 because its j-DOF (vertical response at midspan) is not involved in that mode (the midspan is a fixed node for Mode 3). Some additional insights regarding the robustness of the two proposed topologies, and with specific regard to the flexibility of the grounded stiffness k_G, are provided in the next sections.

5 | PERFORMANCE SENSITIVITY ANALYSIS REGARDING THE PERFECTLY GROUNDED ASSUMPTION FOR FIXED TMDI PARAMETERS

As already stated, a sensitivity analysis has been conducted to investigate what is the role and the effect of simplified assumptions made in Step 2 of the procedure. The focus here is on the assumption of perfectly grounded TMDI, which is common in literature for a wide range of applications. For footbridges, and under the conceptual design layouts shown in Figure 14, perfection in grounded restrains means $k_G = \infty$, something that is hard to realize by the diagonal members in the figure, and also, when realized in practice in the as-built configuration by large values provided for k_G, deterioration effects can lead with time, to nonperfectly grounded configurations. Then, a sensitivity analysis of the comfort performances, at varying values of k_G is performed for the two optimal design solutions presented above in the paper and for different values of the diagonal members' inclination (α in Figure 14). The parameters of the TMDI (b, m_T, k_T, and c_T) are fixed to the optimal values obtained during the optimization carried out by implementing the perfectly grounded assumption, while the reported k_G is intended as the axial stiffness of each of the diagonal members converging to the inerter terminal k as schematized in Figure 14. In order to conveniently show the dependence of the performances from the stiffness of the grounded connection, the nondimensional stiffness parameter λ, defined as the ratio between total stiffness of the grounded TMDI connection and the total stiffness of the TMDI, is introduced. For the topology (a) of Figure 14 (TMDI optimized for Mode 4), it results $\lambda = 2k_G/k_T$, while for topology (b) (TMDI optimized for Mode 3), λ is defined as $\lambda = 4k_G/k_T$.

5.1 | Performance sensitivity curves

General results of the sensitivity analysis are shown in Figure 19 in terms of trends of normalized FRFs for accelerations versus the λ for three different inclinations α denoted with different colors of the curves in the figure, such a curve can be interpreted as "performance sensitivity curves."

From the figure, it can be argued that the efficiency (stiffness) of the TMDI grounded connection can highly affect the performance of the controlling system, leading in the examined case up to 10 times performances detriment when the TMDI is optimally designed for Mode 4 (Figure 19a), and the λ values switch from 10^3 to 10^1 at $\alpha = 4.3°$. It is worth noting that the trend of the curves show a relatively small range of λ values in which there is a significant performance sensitivity, as denoted from the high slope of the curves in that range. For example, for the case of TMDI optimally designed for Mode 4 and $\alpha = 1.4°$ (Figure 19a, blue line), the "performances sensitivity range" is $5{\cdot}10^1 < \lambda < 4{\cdot}10^3$, where the slope of the curve is significant, while for $\lambda < 5{\cdot}10^1$ or $\lambda < 4{\cdot}10^3$, the performance sensitivity curve reaches asymptotic values (almost zero slope) denoting inefficient and efficient vibration control performances, respectively.

As a general consideration, it can be stated that the variation of λ in the examined range of values completely changes the efficiency/behavior of the system, and that the sensitivity to this parameter is then very high.

Since, as already stated, in the performed analysis the TMDI design parameters (b, m_T, k_T, and c_T) are fixed to the optimal values found during the optimization phase (carried out with the perfectly grounded assumption), by varying λ, we are examining a control system that goes away from its optimal configuration by changing its frequency. In addition, by dropping the λ value, we decrease the level of involvement of the inerter in the dynamics, until the limit configuration with $\lambda = 0$, in which the inerter is no more involved in the dynamics due to the inability of the connection to fix the grounded node and then to generate any relative accelerations between the two inerter terminals. As a result, at $\lambda = 0$, we are seeing the response of the footbridge provided with a detuned, nonoptimal low-mass TMD device ($\mu = 0.001$ in the examined case, as indicated in Table 4).

In dropping the λ value, and gradually switching from the performances corresponding to the optimal-designed perfectly grounded TMDI, to the one corresponding to a nonoptimal TMD (again, the inerter is not involved in the dynamic due to the λ, i.e., k_G, ineffectiveness), the devices pass through intermediate configurations, each one representing a nonperfect TMDI (TMDI_{NP}). These aspects are indicated in the figure by highlighting the λ ranges corresponding to the three devices.

The effectiveness of certain diagonal members in perfectly grounding the inerter is, as expected, also depending to α: larger inclinations needs lower values of λ to reach the intended perfection in the grounded restrain. Referring to Figure 19, it can be said that in order to obtain performances comparable with the case $\lambda \to \infty$, it is necessary to have values of $\lambda \approx 1000$ when $\alpha = 1.4°$, but for the larger angles (e.g., $\alpha = 4.3°$ in Figure 19), it is possible to realize a sufficiently rigid connections with $\lambda \approx 100$. On the other side, also if larger inclinations are characterized by lower sensitivities (lower slope of the curves in the performances sensitivity range), the performance sensitivity range enlarges at

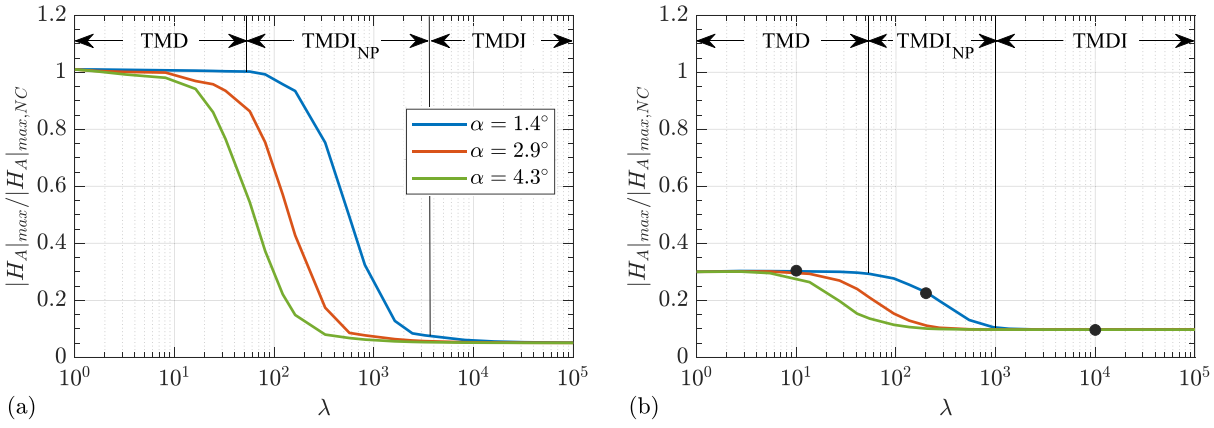

FIGURE 19 Normalized peak value of acceleration FRFs under a harmonic force at varying axial stiffness for the diagonal members connecting the TMDI to the ground: (a) at $L/2$ and force applied at midspan and TMDI optimally designed for Mode 4 ($\lambda = 2k_G/k_T$) and (b) at $L/4$ and force applied at $L/4$ and TMDI optimally designed for Mode 3 ($\lambda = 4k_G/k_T$)

lower inclinations; these behaviors are more evident in Figure 19b (TMDI is optimally designed for Mode 3 and topology (b) in Figure 14).

5.2 | Multimodal control sensitivity

In order to shed further light on the effect of an imperfect ground connection on the performances, the acceleration FRFs for the vertical response at $L/4$ span or at midspan under an harmonic force applied at $L/4$ span, when the footbridge is equipped with the TMDI in topology (b) of Figure 14, and optimized (under the perfectly grounded assumption) for Mode 3, are shown in Figure 20 as obtained for the different values of λ (indicated with dots in Figure 17b) and at $\alpha = 1.4°$.

In the figures, $\lambda = 10^1$ means ineffective connection (nongrounded) and then nonoptimal conventional (low mass) TMD, $\lambda = 2{\cdot}10^2$ means nonperfect TMD (TMDI_{NP}), and finally, $\lambda = 10^4$ means TMDI (with perfect grounded connections), in the same figure, the FRF obtained for the footbridge without any control device (NC case) is also shown for comparison purposes (shaded line), with indication of the mode numbers corresponding to the different peaks.

From the figure, it is clear how the effectiveness of the grounded connection is key for allowing the multimodal control skill of the TMDI. In Figure 20a, it can be seen that, in addition to the perfectly grounded TMDI, both the case of nonconventional–nonoptimal TMD ($\lambda = 10^1$) and nonprefect control system TMDI_{NP} ($\lambda = 2{\cdot}10^2$) are able to drop the peak corresponding to Mode 3, while they do not significantly drop other modal peaks (Modes 2, Mode 4, and higher modes). In some cases (e.g., peak of Mode 4), the effect of a nonperfect connection ($\lambda = 10^1$ or $\lambda = 2{\cdot}10^2$) to the ground is detrimental for the performances, being the peak of the NC structure, lower than the peaks of nonperfect or ineffective grounded connection. On the contrary, in the perfectly grounded TMDI ($\lambda = 10^4$), the multimodal vibration suppression is enabled for Mode 2, Mode 4, and higher modes. The effect is also evident in Figure 20b (vertical acceleration FRF at midspan) where the peak corresponding to Mode 3 does not appear (the midspan is a fixed point for this mode).

The analysis of the FRFs at different λ values allows to highlight a merit of the TMDI with respect to the classical TMD that has been never evidenced in the literature and that appears for the topology (b) of Figure 14 in this study: also, if the grounded connection stiffness of a "perfectly grounded" optimal TMDI having a very low gravitational mass ratio ($\mu = 0.001$ in the examined case) completely deteriorates or is lost during the lifetime of the structure, the performances of the resulting system will be still acceptable ("tuned" mode is dropped). On the contrary, when we use classical TMDs, in order to have the same nominal optimal performances of the optimal (very low mass) TMDI, the gravitational mass will certainly be greater than the one of the TMDI, something which can negatively impact on the performances in case of deterioration or damage of the device. In other words, it can be stated that, if we consider a damage or a deterioration scenario for the device in the design, the low-mass ratios required by the TMDI render it, in principle, more suitable than the TMD because, in noneffective configurations, it has lower impact on the system dynamics. It is important to say here that this consideration has been validated only with reference to the

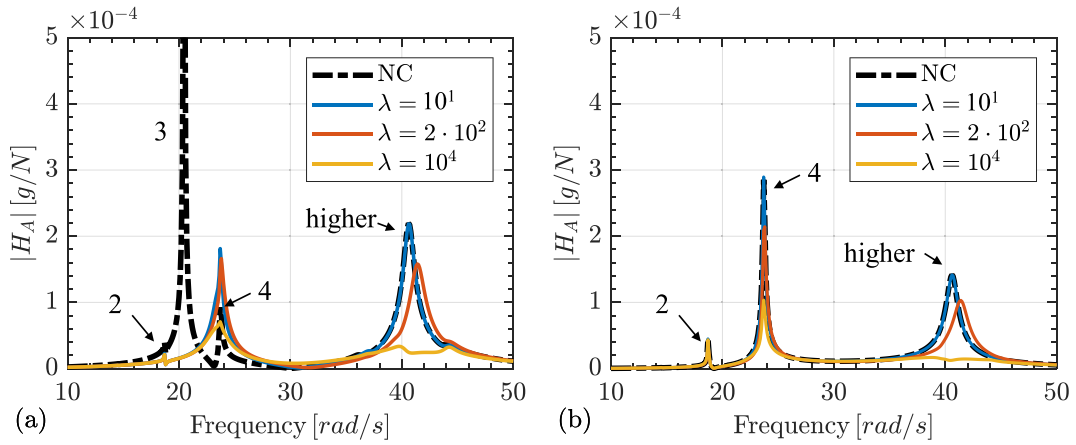

FIGURE 20 Acceleration FRFs at (a) $L/4$-span and (b) midspan. The FRFs are obtained under a harmonic force applied at $L/4$-span and when the design of the TMDI is optimized for Mode 3—topology (b) in Figure 14, at $\alpha = 1.4°$

noneffectiveness of the grounded connection; in order to generalize it, further studies should be carried out the sensitivity of the performances with respect to other parameters.

6 | CONCLUSIONS

A complete procedure for the optimal design of ideal (inerter) and perfectly grounded TMDIs for the comfort performances improvement of footbridges is presented and applied to an existing case-study structure. The proposed TMDI optimal design procedure is feasible and effective and refers to guidelines used by practitioners for footbridges design.

The following conclusions can be made:

- *Use of the TMDI for vibration suppression in footbridges*. In the authors' knowledge, the present paper is the first proposing such an application for the TMDI. Due to the specific characteristics of their dynamic behavior, that is, low damping and multimodal importance in acceleration response, the TMDI is, in principle, particularly suitable as a passive vibration control device for footbridges.
- *Optimal TMDI design procedure for performance improvements*. The proposed procedure is simple (because it is based on generalized SDOF systems), reliable (because it is independent from the structural damping, which is one of the most uncertain parameters in footbridge), and practice oriented (because it is conform with the HiVoSS guidelines that are a standard for practitioners).
- *Application to an existing structure*. The procedure has been applied to an existing footbridge, and performances of the optimal design configuration have been assessed by a three-dimensional MDOF FE model of the structure that has been accurately calibrated by field measurements carried out on the bridge. The application to a real structure of the procedure and the subsequent performance assessment emphasized the practicability of the procedure and allows to assess the reliability of the simplified models (SDOF based) used in the design phase.
- *Considerations for practical implementation of the device*. The proposed SDOF-based optimal design procedure provides more than one optimal solution. Pertinent criteria are then provided and discussed to choose the best optimal solution for its implementation. Such a criteria must be based not only on the vibration suppression level obtained by the optimal solution but also on practical feasibility aspects such as robustness, realization complexity, costs, and durability of the optimal solutions.
- *Effect of imperfections in the grounded connection*. The effect of deviations from the initial assumption of perfectly grounded device has been investigated by a parametric sensitivity analysis and by varying the stiffness of the connection between the TMDI and the ground. In authors' knowledge, the present paper is the first one that carries out this kind of investigation. It results that a nonperfect (low stiffness) connection of the TMDI to the ground can drop the performances of the TMDI in suppressing the vibrations up to the complete vanishing of its beneficial effects. It is possible to individuate the stiffness lower values that must not be provided for realizing a perfect connection. As a further development of the research, it can be said that in the case that it is not possible to achieve a perfect connection of the TMDI system to the ground, the optimal design procedure should consider the λ parameter as a design variable in the optimization phase. It is worth noting that the above considerations have general validity for any application of the TMDI which considers grounded connections.

It can be said that, in general, the TMDI is shown to be a high-performing device for suppressing excessive vibrations for footbridges in order to improve comfort performance.

Regarding the case study analyzed in the paper, it can be concluded that between the two proposed topologies for practical implementation of the TMDI, the best is the one identified as (b) in Figure 14: two TMDI attached at $L/4$ and a $3/4L$ along the deck. This configuration is shown to be more efficient and more robust of the topology (a), especially with respect to the ineffectiveness of the grounded connection as shown in the last section of the paper.

ACKNOWLEDGMENTS

The cooperation agreement with Municipality of Rieti and financial support of Sapienza Università di Roma under Grants RM11715C8262BE71 (financial framework 2017) and RP1181643697C751 (financial framework 2018) are gratefully acknowledged. Fruitful discussions with Dr. Agathoklis Giaralis from City University of London regarding the TMDI and its behavior are gratefully acknowledged.

AUTHOR CONTRIBUTIONS

Maurizio De Angelis: Original idea, Conceptualization, Review of the numerical results and review of the text. Francesco Petrini: Conceptualization, Review of the numerical results and writing of the text. Daniele Pietrosanti: Numerical analyses and review of the text.

ORCID

Maurizio De Angelis https://orcid.org/0000-0003-1896-3705
Francesco Petrini https://orcid.org/0000-0002-9477-110X

REFERENCES

1. Van Nimmen K, Lombaert G, De Roeck G, Van den Broeck P. Vibration serviceability of footbridges: evaluation of the current codes of practice. *Eng Struct*. 2014;59:448-461.
2. Ricciardelli F, Demartino C. Design of footbridges against pedestrian-induced vibrations. *J Bridge Eng*. 2016;21(8):1-3, C4015003.
3. Caetano E, Cunha Á, Moutinho C, Magalhães F. Studies for controlling human-induced vibration of the Pedro e Inês footbridge, Portugal. Part 2: implementation of tuned mass dampers. *Eng Struct*. 2010;32(4):1082-1091.
4. Li Q, Fan J, Nie J, Li Q, Chen Y. Crowd-induced random vibration of footbridge and vibration control using multiple tuned mass dampers. *J Sound Vib*. 2010;329(19):4068-4092.
5. Venuti F, Reggio A. Mitigation of human-induced vertical vibrations of footbridges through crowd flow control. *Struct Control Health Monit*. 2018;25(12):1-16, e2266. https://doi.org/10.1002/stc.2266
6. Terrill R, Bäumer R, Van Nimmen K, Van den Broeck P, Starossek U. Twin rotor damper for human-induced vibrations of footbridges. *J Struct Eng*. 2020;146(7):1-16, 04020119. https://doi.org/10.1061/(asce)st.1943-541x.0002654
7. Smith MC. Synthesis of mechanical networks: the inerter. *IEEE Trans Automat Control*. 2002;47(10):1648-1662.
8. Pietrosanti D, De Angelis M, Giaralis A. Experimental study and numerical modeling of nonlinear dynamic response of SDOF system equipped with tuned mass damper inerter (TMDI) tested on shaking table under harmonic excitation. *Int J Mech Sci*. 2020;184:105762. https://doi.org/10.1016/j.ijmecsci.2020.105762
9. Wang FC, Hong MF, Lin TC. Designing and testing a hydraulic inerter. *Proc Inst Mech Eng C J Mech Eng Sci*. 2011;1(265):66-72.
10. Gonzalez-Buelga A, Clare LR, Neild SA, Jiang JZ, Inman DJ. An electromagnetic inerter-based vibration suppression device. *Smart Mater Struct*. 2015;24(5):1-10, 055015. https://doi.org/10.1088/0964-1726/24/5/055015
11. Marian L, Giaralis A. Optimal design of a novel tuned massdamper-inerter (TMDI) passive vibration control configuration for stochastically support-excited structural systems. *Prob Eng Mech*. 2014;38:156-164.
12. De Angelis M, Perno S, Reggio A. Dynamic response and optimal design of structure with large mass ratio TMD. *Earthq Eng Struct D*. 2012;41(1):41-60.
13. Reggio A, De Angelis M. Optimal energy-based seismic design of non-conventional Tuned Mass Damper (TMD) implemented via inter-story isolation. *Earthq Eng Struct D*. 2015;44(10):1623-1642.
14. Pietrosanti D, De Angelis M, Basili M. Optimal design and performance evaluation of systems with Tuned Mass Damper Inerter (TMDI). *Earthq Eng Struct D*. 2017;46(8):1367-1388.
15. Dai J, Xu ZD, Gai PP. Tuned mass-damper-inerter control of wind-induced vibration of flexible structures based on inerter location. *Eng Struct*. 2019;199:1-15, 109585. https://doi.org/10.1016/j.engstruct.2019.109585
16. Petrini F, Giaralis A, Wang Z. Optimal tuned mass-damper-inerter (TMDI) design in wind-excited tall buildings for occupants' comfort serviceability performance and energy harvesting. *Eng Struct*. 2020;204:1-16, 109904. https://doi.org/10.1016/j.engstruct.2019.109904
17. Giaralis A, Petrini F. Wind-induced vibration mitigation in tall buildings using the tuned mass-damper-inerter. *J Struct Eng*. 2017;143(9):1-11, 04017127. https://doi.org/10.1061/(asce)st.1943-541x.0001863
18. De Angelis M, Giaralis A, Petrini F, Pietrosanti D. Optimal tuning and assessment of inertial dampers with grounded inerter for vibration control of seismically excited base-isolated systems. *Eng Struct*. 2019;196:1-19, 109250. https://doi.org/10.1016/j.engstruct.2019.05.091
19. Giaralis A, Taflanidis AA. Optimal tuned mass-damper-inerter (TMDI) design for seismically excited MDOF structures with model uncertainties based on reliability criteria. *Struct Control Health Monit*. 2018;25(2):1-22, e2471. https://doi.org/10.1002/stc.2082
20. Taflanidis AA, Giaralis A, Patsialis D. Multi-objective optimal design of inerter-based vibration absorbers for earthquake protection of multi-storey building structures. *J Franklin Inst*. 2019;356(14):7754-7784.
21. De Domenico D, Ricciardi G. An enhanced base isolation system equipped with optimal tuned mass damper inerter (TMDI). *Earthq Eng Struct D*. 2018;47(5):1169-1192.
22. Xu K, Bi K, Han Q, Li X, Du X. Using tuned mass damper inerter to mitigate vortex-induced vibration of long-span bridges: analytical study. *Eng Struct*. 2019;182:101-111.
23. Sarkar S, Fitzgerald B. Vibration control of spar-type floating offshore wind turbine towers using a tuned mass-damper-inerter. *Struct Control Health Monit*. 2020;27(1):1-23, e2471. https://doi.org/10.1002/stc.2471
24. Fujino Y, Siringoringo DM. A conceptual review of pedestrian-induced lateral vibration and crowd synchronization problem on footbridges. *J Bridge Eng*. 2016;21(8):1-12. https://doi.org/10.1061/(asce)be.1943-5592.0000822

25. Živanovic S, Pavic A, Reynolds P. Probability-based prediction of multi-mode vibration response to walking excitation. *Eng Struct*. 2017; 29(6):942-954.
26. Van Nimmen K, Lombaert G, De Roeck G, Van den Broeck P. The impact of vertical human-structure interaction on the response of footbridges to pedestrian excitation. *J Sound Vib*. 2017;402:104-121.
27. Tubino F, Piccardo G. Serviceability assessment of footbridges in unrestricted pedestrian traffic conditions. *Struct Infrastruct E*. 2016; 12(12):1650-1660.
28. Bruno L, Venuti F. Crowd-structure interaction in footbridges: modelling, application to a real case-study and sensitivity analyses. *J Sound Vib*. 2009;323(1–2):475-493.
29. Bassoli E, Van Nimmen K, Vincenzi L, Van den Broeck P. A spectral load model for pedestrian excitation including vertical human-structure interaction. *Eng Struct*. 2018;156:537-547.
30. Brownjohn JMW, Pavic A, Omenzetter P. A spectral density approach for modelling continuous vertical forces due to walking. *Can J Civil Eng*. 2004;31(1):65-77.
31. Venuti F, Racic V, Corbetta A. Modelling framework of pedestrian-footbridge interaction in vertical direction. *Proc Eng*. 2017;199: 2901-2906.
32. Tubino F. Probabilistic assessment of the dynamic interaction between multiple pedestrians and vertical vibrations of footbridges. *J Sound Vib*. 2018;417:80-96.
33. Tubino F, Pagnini L, Piccardo G. Uncertainty propagation in the serviceability assessment of footbridges. *Struct Infrastruct E*. 2020;16(1): 123-137.
34. Research Fund for Coal and Steel, 2008. HiVoSS: design of footbridges; Report: Research Fund for Coal and Steel 2007, Project RFS2-CT-2007-00033.
35. Gheitasi A, Ozbulut OE, Usmani S, Alipour M, Harris DK. Experimental and analytical vibration serviceability assessment of an in-service footbridge. *Case Studies in Nondestructive Testing and Evaluation*. 2016;6(Part A):79-88.
36. Pietrosanti D, De Angelis M, Basili M. A generalized 2-DOF model for optimal design of MDOF structures controlled by Tuned Mass Damper Inerter (TMDI). *Int J Mech Sci*. 2020;185:105849. https://doi.org/10.1016/j.ijmecsci.2020.105849

How to cite this article: De Angelis M, Petrini F, Pietrosanti D. Optimal design of the ideal grounded tuned mass damper inerter for comfort performances improvement in footbridges with practical implementation considerations. *Struct Control Health Monit*. 2021;e2800. https://doi.org/10.1002/stc.2800

APPENDIX A

Consider a primary structure modeled as a MDOF system having N-degrees of freedom to be controlled by a TMDI. The TMDI consists of a mass m_T connected to the j level of the MDOF structure by a linear spring of stiffness k_T and a viscous damper of damping coefficient c_T and connected to the ground by an inerter device of inertance b. The resultant system has $N + 1$-DOF.

The equations of motion for such a structure subject to external vector force $\mathbf{f}$ are

$$\begin{gathered}\mathbf{M}\ddot{\mathbf{u}} + \mathbf{L}\dot{\mathbf{u}} + \mathbf{K}\mathbf{u} = \mathbf{B}_f\,\mathbf{f} + f_B + \mathbf{B}_j f_T \\ m_T\ddot{u}_T = -m_T\ddot{u}_g - f_B - f_T \\ f_B = b\ddot{u}_T \quad f_T = c_T\left(\dot{u}_T - \dot{u}_j\right) + k_T\left(u_T - u_j\right)\end{gathered} \tag{A1}$$

where $\mathbf{M}$, $\mathbf{L}$, and $\mathbf{K}$ represent the $(N \times N)$ mass, damping, and stiffness matrices, respectively; $\mathbf{u}$ is the $(N \times 1)$ displacement vector relative to the ground; u_T is the relative displacement of the mass m_T with respect to the ground; and u_j is the relative displacement of j-DOF with respect to the ground. f_B is the inerter force acting on the ground, and f_T is the viscoelastic force acting on the j-DOF; finally, $\boldsymbol{B}_f$ is the $(N \times N)$ allocation matrix of external force, $\mathbf{B}_j$ is the $(N \times 1)$ allocation vector of viscoelastic force, and dots over symbols represent time derivatives.

By assuming the MDOF structure as classically damped, the displacement vector $\mathbf{u}$ can be approximated as $\mathbf{u}(t) = \boldsymbol{\phi}\, u_j(t)$, where $\boldsymbol{\phi}$ is a vibration shape vector, normalized to have the j element unitary ($\phi_j = 1$), and u_j is the relative displacement of the j-DOF. Under this assumption, a generalized 2-DOF system is introduced, as illustrated in Figure 5.

Table A1 shows how to relate the dynamic properties and response quantities of the generalized 2-DOF system with those of the $N + 1$-DOF system.

TABLE A1 Dynamic properties and response quantities and of the generalized 2-DOF system

Parameter	*N*-DOF + TMDI system	SDOF + TMDI system
Mass	$\boldsymbol{\phi}^T\mathbf{M}\boldsymbol{\phi}$	m_I
Damping coefficient	$\boldsymbol{\phi}^T\mathbf{L}\boldsymbol{\phi}$	c_I
Stiffness	$\boldsymbol{\phi}^T\mathbf{K}\boldsymbol{\phi}$	k_I
Displacement	$u_j(t)$	$u_I(t)$
External force	$\boldsymbol{\phi}^T\mathbf{B}_j\mathbf{f}(t)$	$p(t)$